

Quantum molecular dynamics study of polaron recombination in conjugated polymers

Mark N. Kobrak* and Eric R. Bittner

Department of Chemistry, University of Houston, Houston, Texas 77204

(Received 1 March 2000)

We examine the dynamics of polaron recombination in conjugated polymer systems using mixed quantum classical molecular dynamics. The model treats the particle-hole pair as a fully correlated two-particle quantum mechanical wave function interacting with a one-dimensional classical vibrational lattice. This description allows a natural evolution of the particle-hole wave function from the polaron limit to the exciton limit, and we have performed real-time simulations of the coupled nuclear and electronic dynamics associated with the scattering of polarons into exciton states. We use these simulations to calculate cross sections for exciton formation as a function of spin state, and explore the variation of these cross sections with respect to changes in the magnitude of the particle-hole Coulomb interaction and the effective masses of the quasiparticles. Our results indicate that for an optimal choice of parameters the electroluminescence quantum yield may be as high as 59%, substantially greater than the 25% predicted by simple spin statistics. We interpret these results in a diabatic framework, and suggest strategies for the design of organic systems for use in electroluminescent devices.

I. INTRODUCTION

Since the publication of the first reports indicating the feasibility of constructing light-emitting diodes (LED's) from conjugated polymers,^{1,2} there has been a great deal of interest in adapting these materials for use in devices. Organic materials offer many potential advantages over inorganic semiconductors, including ease of fabrication and favorable mechanical properties.^{3,4} However, the relatively low electroluminescence efficiency of organic materials in LED's has limited their utility,^{3,5} and as a consequence considerable experimental effort has been devoted to the discovery of more efficient polymer systems.⁶⁻⁸ While these efforts have led to significant improvements in the electroluminescence quantum efficiency in test devices, the investigation of new materials remains an active area of research.

From a theoretical standpoint, the process of photoemission from a LED may be divided into three parts. The first is the collision between oppositely charged polarons, the second is the scattering of those polarons into exciton states, and the third is the transition to the ground electronic state, either by radiative or nonradiative decay processes. The importance of understanding the likelihood of a collision stems from the fact that photoemissive states are quenched by proximity to the conductive electrode surface such that any recombination event near the surface represents a loss of fluorescence yield.³ A number of theoretical studies have examined the likelihood of collisions in the bulk polymer under various conditions,⁹⁻¹² and the process has been found to be sensitive to parameters such as the charge carrier density and mobility, the strength of the external field, and the morphology of the polymer sample.

Much less is known about the scattering and decay stages of the recombination process, and one of the most critical questions concerns the spin state of the exciton. Transitions between the triplet exciton states and the ground electronic state are dipole-forbidden, and the predominant decay pathways are therefore non-radiative. Thus, to a first approxima-

tion, any scattering events leading to the formation of triplet exciton states represent a loss of electroluminescence quantum efficiency. Since the exciton spin space includes one singlet state and three triplet states, a statistical distribution of spin states would lead to a maximum quantum electroluminescence quantum efficiency Φ_{EL}

$$\Phi_{EL} = \Phi_{PL}/4 \quad (1.1)$$

where Φ_{PL} is the photoluminescence quantum efficiency.^{3,10}

This statistical argument neglects the possibility that singlet and triplet exciton states may have different cross sections with respect to formation, and ignores the possibility of transitions between triplet and singlet electronic states (i.e., intersystem crossing). Recent measurements by Cao *et al.*¹³ on the output of a light-emitting diode based on electroluminescence from a derivative of poly(*p*-phenylene vinylene) indicated that the ratio Φ_{EL}/Φ_{PL} may be as high as 50%. To understand this result, one must move beyond the statistical approximation and examine the details of the recombination process.

With regard to the decay process, Burin and Ratner⁵ have constructed a master equation approach in which both radiative and non-radiative decay pathways are included for each state. Their results indicate that the existence of triplet to singlet crossings in the relaxation of oligothiophenes significantly affects Φ_{EL} , though it does not increase it above the statistical limit of $\Phi_{PL}/4$. The Burin and Ratner model does not contain any information on the details of the scattering process, however, and other theoretical treatments of polaron recombination have treated the process purely phenomenologically.⁹⁻¹² The difficulty in modelling the scattering process itself lies in the fact that the transition from polaronic to excitonic states requires simultaneous solution of both vibrational and electronic dynamics. Conventional calculations of this type are difficult even for small molecules,¹⁴⁻¹⁶ and rapidly become prohibitive in extended polymeric systems.

TABLE I. Potential energy parameters employed in this work.

$V_C(x_p - x_h) = \frac{-Ux_0}{\sqrt{x_0^2 + (x_p - x_h)^2}}$	$U = 2.72 \text{ eV}, x_0 = 1.75 \text{ \AA}$
$T_i = -\mathbf{p}_i^2/2m_i$	$m_p = m_h = 1 \text{ emu}$
$V_{i\text{-latt}} = \sum_j A_j \exp[-B(x_i - R_j)^2]$	$A_p = -5.697 \text{ eV}, A_h = 5.263 \text{ eV}$
	$B = 0.7439 \text{ \AA}^{-2}$
$V_e = e_i \mathcal{E} x_i$	$\mathcal{E} = -8.919 \times 10^{-4} \text{ eV/\AA}, e_p = -1, e_h = +1$
$V_{2r} = \frac{-U_r x_0}{\sqrt{x_0^2 + (x_p - x_h)^2}}$	$U_r = -1.24 \times 10^{-2} \text{ eV}$
$V_b = C(\exp[-(x - x_a)^2/\sigma^2] + \exp[-(x - x_b)^2/\sigma^2])$	$C = 2.48 \text{ eV}, \sigma = 2.77 \text{ \AA}$
	$\{x_a, x_b\}$ are grid boundaries

We have recently constructed a methodology based on the particle-hole picture of solid-state physics that allows the simulation of the vibronic dynamics of an extended one-dimensional polymer system. In this approach, the electronic degrees of freedom are modelled as a fully quantum-mechanical particle-hole pair, which is self-consistently coupled to a classical vibrational lattice representing the polymer backbone. In the present work, we extend this theory and carry out quantum molecular dynamics simulations of the formation of excitonic states from polarons, and calculate cross sections for the formation of singlet and triplet excitons as a function of exciton binding energy and the strength of the applied voltage bias. Our approach does not address the question of the probability that two polarons will encounter each other in the bulk material, but begins with two oppositely charged polarons already present on a single conjugation domain. The time-dependent equations of motion are then numerically integrated and the polaron interaction is treated explicitly.

II. HAMILTONIAN FOR USE IN POLARON RECOMBINATION

A. Relationship between parity and spin state

Our goal is to develop a formalism that will allow us to treat the recombination of polarons into excitons. We write the particle-hole wave function $|\psi\rangle$ as

$$|\Psi\rangle = \sum_{ij} c_{ij} |ij\rangle |\chi\rangle, \quad (2.1)$$

where i and j are particle and hole states, respectively, and $|\chi\rangle$ is the spin state for the particle-hole pair (singlet or triplet). These are given in Ref. 17 as

$$|1,1\rangle = |\alpha_v \alpha_c\rangle, \quad (2.2)$$

$$|1,-1\rangle = |\beta_v \beta_c\rangle, \quad (2.3)$$

$$|1,0\rangle = \frac{1}{\sqrt{2}} (|\beta_v \alpha_c\rangle + |\alpha_v \beta_c\rangle), \quad (2.4)$$

$$|0,0\rangle = \frac{1}{\sqrt{2}} (|\beta_v \alpha_c\rangle - |\alpha_v \beta_c\rangle), \quad (2.5)$$

where the state $|i, j\rangle$ denotes the spin and angular momentum quantum number, α and β denote spin up and spin down for the individual quasiparticles, and the subscripts v and c indicate whether the quasiparticle is in the conduction or the valence band (particle or hole, respectively).

The Hamiltonian is given by Cho,¹⁸ and may be written as

$$H = \hat{h}_p + \hat{h}_h + \hat{V}_2, \quad (2.6)$$

where \hat{h}_p and \hat{h}_h are the one-body Hamiltonians for the particle and hole, respectively, which include both the kinetic energy of each quasiparticle and the potential energy for their interaction with the lattice. \hat{V}_2 is the potential energy of interaction between the particle and hole, given as

$$\hat{V}_2 = \frac{1}{2} \sum_{klmnq} |q\rangle \langle kl| \langle kl| \langle q| V_C(x_p - x_h) \times (\hat{1} - \hat{X}) |q\rangle |mn\rangle \langle mn| \langle q|, \quad (2.7)$$

where $k, l, m,$ and n are indices over coordinate space basis functions, and q is an index over spin state (singlet or triplet). $V_C(x)$ is the Coulombic attraction between the particle and hole. This is modeled as an Ohno potential with parameters given in Table I.¹⁷ The exchange operator, \hat{X} , swaps the labels on the particle and hole,

$$\hat{X} |\Psi\rangle = \sum_{ij} c_{ij} \hat{X} |ij\rangle |\chi\rangle = (-1)^Q \sum_{ij} c_{ij} |ji\rangle |\chi\rangle, \quad (2.8)$$

where Q is the spin (0 or 1) for the state $|\chi\rangle$. The negative sign arises from the fact that the triplet spin state is antisymmetric under exchange of the particle and hole, while the singlet state is symmetric.¹⁹

Let us recast the wave function in coordinate space

$$|\Psi\rangle = \sum_{ij} c_{ij} |ij\rangle |\chi\rangle = \int dx_p dx_h \psi(x_p, x_h) |x_p\rangle |x_h\rangle |\chi\rangle. \quad (2.9)$$

The coordinate space projection of the wave function is now contained in $\psi(x_p, x_h)$. A similar operation on the wave function after exchange yields

$$\begin{aligned}\hat{X}|\Psi\rangle &= (-1)^Q \sum_{ij} c_{ij} |ji\rangle |\chi\rangle \\ &= (-1)^Q \int dx_p dx_h \psi(x_h, x_p) |x_p\rangle |x_h\rangle |\chi\rangle.\end{aligned}\quad (2.10)$$

Thus exchange of the indices on the particle and hole is equivalent to swapping the axes x_p and x_h in coordinate space.^{17,20}

Using this coordinate space representation, the expectation value for the particle-hole interaction energy E_2 may be written

$$\begin{aligned}E_2 &= \frac{1}{2} \int dx_p dx_h \psi^*(x_p, x_h) V_C(x_p - x_h) \\ &\quad \times [\psi(x_p, x_h) + (-1)^{(Q+1)} \psi(x_h, x_p)],\end{aligned}\quad (2.11)$$

where we have assumed the spin of the system is a pure state. This implies that for $Q=1$, $E_2=0$ unless $\psi(x_1, x_2) = \psi(x_2, x_1)$, and for $Q=0$, $E_2=0$ unless $\psi(x_1, x_2) = -\psi(x_2, x_1)$. In other words, only components of $\psi(x_p, x_h)$ which are symmetric across the line $x_p = x_h$ may be bound in a triplet spin state, and only components of $\psi(x_p, x_h)$ which are antisymmetric across the line $x_p = x_h$ may be bound in a singlet spin state.

To understand the implications of this restriction, we must look more closely at the one-body terms, \hat{h}_p and \hat{h}_h . These may be written

$$\begin{aligned}\hat{h}_p &= T_p + V_{p\text{-latt}} - V_e(x_p), \\ \hat{h}_h &= T_h + V_{h\text{-latt}} + V_e(x_h),\end{aligned}\quad (2.12)$$

where T_i is the kinetic energy operator for the i th quasiparticle and $V_{i\text{-latt}}$ is the interaction between the quasiparticle and the lattice sites. The construction of these terms is given in Ref. 17. $V_e(x)$ represents an interaction between the quasiparticle and an external electric field representing an applied voltage gap across the polymer which drives electroluminescence. We assume a linear electric field with a magnitude comparable to that employed by Conwell and Wu²¹ in their simulations. The functional forms for each of these terms are given in Table I.

The sum of the one-body operators, $\hat{H}_1 = \hat{h}_h + \hat{h}_p$, can be decomposed into operators which are symmetric and anti-symmetric under the exchange operation, $\hat{H}_1 = \hat{H}_{1s} + \hat{H}_{1a}$. In a system where charge conjugation symmetry is preserved, $\hat{H}_{1a} = 0$ and the Hamiltonian is invariant under the exchange operation. However, the nonlinear form of the quasiparticle-lattice coupling breaks charge conjugation symmetry in the polaron limit,^{22,23} as does the presence of the electric field. The breaking of charge conjugation symmetry has been experimentally confirmed in polaron states in conjugated polymer systems.^{24,25} Therefore, rather than restricting the symmetry of the wavefunction in the exciton limit as we did in our previous work,¹⁷ here we explicitly include the direct and exchange terms of the Coulomb potential given in Eq. (2.11). This implies that a triplet (singlet) exciton will contain some contribution from antisymmetric (symmetric) states. How-

ever, the energy gap between bound states of \hat{V}_2 is much larger than the values of H_{1a} so this effect will be negligible in the exciton limit.

Finally, it will prove convenient to define the total potential energy of the particle-hole pair as

$$\begin{aligned}V_{\text{QM}}(x_p, x_h, \mathbf{R}) &= V_C(x_p - x_h) + V_{p\text{-latt}}(x_p, \mathbf{R}) + V_{h\text{-latt}}(x_h, \mathbf{R}) \\ &\quad - V_e(x_p) + V_e(x_h).\end{aligned}\quad (2.13)$$

In Sec. III, we interpret polaron scattering within a diabatic framework, and V_{QM} plays a key role in such a discussion.

B. Treatment of the spin state

Having outlined the treatment of the wavefunction in coordinate space, we now address the treatment of the spin degrees of freedom. In the limit of asymptotic separation between the particle and hole, the singlet and triplet spin states are degenerate. However, as the particle and hole approach each other, the exchange term in Eq. (2.7) breaks the degeneracy.

In principle, the framework outlined here permits the possibility of scattering between singlet and triplet spin states. In practice, implementing such a calculation requires the simultaneous propagation of multiple two-body coordinate space wave functions, one corresponding to each spin state, with spin-orbit interactions coupling the wave functions. Transitions between states of singlet and triplet symmetry are ubiquitous in conjugated systems,^{5,26} but are generally mediated by a doubly-excited singlet state such as the 2^1A_g state of polyenes.²⁶ McClure has shown²⁷ that singlet-triplet transitions for states of B_u symmetry in π -conjugated systems are very weak, and that the magnitude of spin-orbit coupling between such states is expected to be less than 1 cm^{-1} . Even in the limit of degenerate singlet and triplet states, this implies a multipicosecond time scale for such transitions which is sufficiently long relative to our calculation that these transitions may be neglected. We instead restrict the wave function to remain in a pure spin state throughout the recombination process, and perform separate simulations for the singlet and triplet states.

Because the spin state does not change during recombination, the probability that a given scattering event will lead to photoemission is determined by the absolute cross sections for exciton formation in singlet and triplet spin states. Let us define the cross section, γ , to be the population in an exciton state after the recombination event for a given set of initial conditions. The probability of emission due to the single scattering event is then

$$\chi_{\text{EL}} = \frac{\gamma_S}{\gamma_S + 3\gamma_T} \Phi_{\text{PL}},\quad (2.14)$$

where γ_S and γ_T are singlet and triplet exciton scattering cross sections, respectively.

Because the process of photoemission is complex, it is worth detailing the relationship between χ_{EL} and the total electroluminescence quantum yield Φ_{EL} . χ_{EL} represents the likelihood that, if two randomly prepared charge carriers come into contact within the bulk material, they will scatter into the singlet manifold. If one assumes that (1) collisions between polarons are uncorrelated (i.e., χ_{EL} is the same for

all collisions in the bulk), (2) loss due to interactions with the electrode surfaces is negligible, and (3) that intersystem crossing is unimportant, then $\chi_{\text{EL}} = \Phi_{\text{EL}}$. All three of these assumptions are inherent in the calculation of the statistical limit on electroluminescence quantum efficiency.³ Indeed, if one makes the additional assumption that the scattering cross-sections for singlet and triplet states are equal ($\gamma_S = \gamma_T$), Eq. (2.14) reduces to the statistical limit $\Phi_{\text{EL}} = \Phi_{\text{PL}}/4$. In Sec. III we calculate the values of γ_S and γ_T , allowing calculation of χ_{EL} for our model system. This value represents an improved estimate on the limit for Φ_{EL} , and is a primary objective of this work.

III. RESULTS AND DISCUSSION

The quantum degrees of freedom representing the particle and hole were represented using a discrete coordinate space grid to allow evaluation of the kinetic energy operator via fast Fourier transform.²⁸ The quantum time evolution operator was calculated via a short iterative Lanczos procedure.²⁹ The nuclear degrees of freedom were modeled as a one-dimensional classical harmonic lattice interacting with the quasiparticle pair, and the coupled quantum and classical equations of motion were simultaneously integrated. Except where noted below, the form of the Hamiltonian and all parameters employed in the calculation were the same as those employed in our previous work.^{17,30}

A. Determination of polaron states

Before we begin studying the recombination of polarons, we must construct an initial state consisting of two widely-separated polarons. We use the same relaxation technique that was used in Ref. 17, in which an imaginary-time propagation of the quantum degrees of freedom is coupled to a kinetically damped propagation of the lattice degrees of freedom.

The grid employed in this calculation is 138 Å long; our goal is to generate two polarons on this grid which are as widely separated as possible without being close enough to the grid boundaries to create artifacts. To this end, we replace the Coulombic interaction \hat{V}_2 between the quasiparticles with a weakly repulsive potential, denoted \hat{V}_{2r} (see Table I), and enforce periodic boundary conditions on the quantum degrees of freedom. \hat{V}_{2r} is therefore present both at the center and the boundary of the grid, insuring the polarons will form halfway between the two limits. While the presence of \hat{V}_{2r} implies an interaction between the quasiparticles, the perturbation is small and the resultant structure for the polarons should be a sufficiently accurate representation of the asymptotic polaron limit for our purposes. As in Ref. 17, the classical degrees of freedom were taken to be periodic across the grid domain, and were kinetically damped such that the resultant configuration for the system corresponded to that of two polarons at $T=0$ K.

The initial quantum wave function was taken to be constant everywhere, $\psi(x_p, x_h) = C$. To insure rapid convergence, the lattice coordinates were displaced from equilibrium such that

$$\Delta R_i = 0.017 \text{ \AA} \sin[2\pi R_{i0}/x_l], \quad (3.1)$$

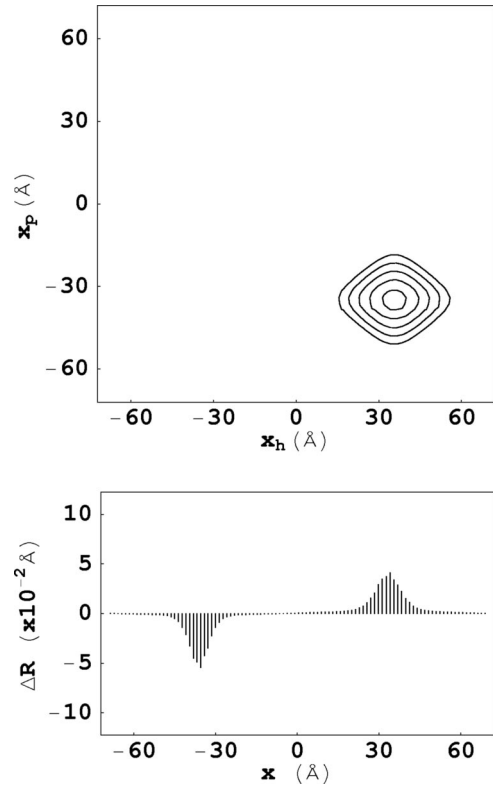


FIG. 1. Configuration of the polaron pair, as described in the text. Top: Probability density distribution in coordinate space for the particle-hole pair. Contour lines are drawn geometrically, such that each line is $4\times$ larger than its neighbor. Bottom: Displacement of each lattice site from its equilibrium, as a function of position.

where R_{i0} is the equilibrium coordinate of the i th lattice site, ΔR_i is its displacement from equilibrium, and x_l is the length of the grid.

The equations of motion were then propagated in imaginary time until the energy converged. The parameters used for exciton-phonon coupling given in Ref. 17 did not produce a satisfactory form for the polarons; the positive (hole) polaron was found to have a width comparable to the size of the grid, much larger than polarons observed in other calculations, where widths were on the order of 5 Å.³¹ The difficulty in our calculation was found to lie in the choice of parameters for the exciton-phonon coupling; the original parameters were based on semi-empirical constants taken from Ref. 32, and when these were replaced with parameters from Ref. 33 a more reasonable form for the polarons was obtained, shown in Fig. 1. The reason for the improvement is likely that whereas the parameters in Ref. 32 were optimized for use in a model which included only nearest neighbor Coulombic interactions between electrons, those in Ref. 33 were optimized for use with a longer-ranged Coulombic interaction based on a screened Ohno potential. The more accurate treatment of electronic correlation effects leads to a better fit for electron-phonon coupling parameters, and thus a better description of the polaron state. We do not expect the change in exciton-phonon coupling to qualitatively affect the results obtained in the exciton limit, however, as the same functional form of the coupling still applies. We determined the total energy for the two asymptotically separated po-

TABLE II. Free polaron configuration data.

	Particle polaron	Hole polaron
x_0	-35.33 \AA	34.04 \AA
RMS width	4.22 \AA	5.16 \AA
Aggregate data for polaron configuration [34]		
$\langle H \rangle$		-1135.3 cm^{-1}
$\langle E_Q \rangle$		-3006.1 cm^{-1}
$\langle V_{\text{latt}} \rangle$		1870.8 cm^{-1}

larons to lie 1135.3 cm^{-1} below the energy of a free particle-hole pair³⁴ in this system (see Table II).

This configuration represents the most stable polaronic structure for our model in the absence of an external electric field. However, the process of electroluminescence takes place in the presence of an electrical potential. We cannot obtain the true form of the polaron in the presence of the field because the energy of the polarons will always be decreased by translation along an electric field, and the true minimum energy polaron state lies at the end of the polymer. However, it is also known that polarons in conjugated polymer systems “hop” between conjugation domains rather than propagating continuously along the polymer,²¹ so that polarons in physical recombination processes may not represent steady-state systems. With these ambiguities in mind, we take the polaron minimum energy configuration *sans* field to be our initial configuration in all the propagations reported here.

B. Simulation of recombination dynamics

In simulations of electroluminescence, the presence of an external electric field introduces an inherent anisotropy to the potential energy, and periodic boundary conditions cannot be employed. This is a particular problem in the propagation of the quantum equations of motion in our system, as the fast Fourier transform algorithm used to evaluate the kinetic energy assumes a periodic form for the wave function.²⁸ We therefore forced the amplitude of the wave function to converge to zero at the grid boundaries by surrounding the grid with a Gaussian barrier $V_b(x)$. One may view the existence of this boundary as a break in the conjugation of the polymer³⁵ which prevents the quasiparticles from freely propagating into neighboring regions of the polymer. In keeping with this description, the classical degrees of freedom were taken to be periodic, but the three lattice sites nearest each end of the polymer were kinetically damped. This eliminated phonons which reached the grid boundaries without introducing unphysical reflections from the terminal atoms; in essence, we have assumed that phonons propagate through conjugation breaks and do not return.

The initial configuration of the system was taken to be the widely-separated polaron pair described above. The potential energy surface, $V_{\text{QM}}(x_p, x_h, \mathbf{R})$, associated with the initial form of the lattice is shown in Fig. 2. The distortion of the lattice creates a potential energy well in the region of $x_p = -30 \text{ \AA}$, $x_h = 30 \text{ \AA}$, in which the initial wave function is localized. This distortion also creates a region which is repulsive to the wave function at $(30, -30)$, owing to the op-

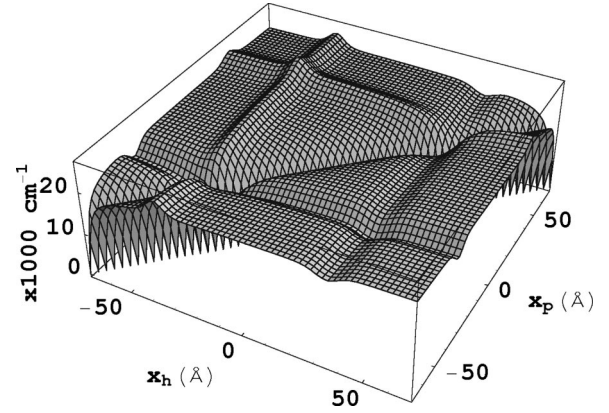


FIG. 2. Potential energy $V_{\text{QM}}(x_p, x_h, \mathbf{R})$ for the initial configuration of the system (assuming favorable exchange interaction).

posite sign of the particle and hole lattice interactions. The potential well created by the Coulomb interaction is centered on the line $x_p = x_h$, and in addition to being deeper than the well associated with the lattice distortion, it also does not restrict the motion of the particle-hole center of mass. Indeed, the free exciton is delocalized along the entire conjugation domain, leading to a high density of exciton states.¹⁷

From this initial configuration, the equations of motion were integrated in time for both the singlet and triplet spin states. With the exception of the sign of the exchange interaction given in Eq. (2.11), the numerical treatment of the two propagations was identical. As expected, the presence of the electric field and the Coulombic attraction between the particle and hole drew the quasiparticles together. As shown in Figs. 3 and 4, the polarons distorted slightly as they propagated, but for the most part retained their configuration; the wave packet remained localized, and the form of the lattice distortion was virtually unchanged at early times.

The dynamics surrounding polaron scattering were similar for both the singlet and triplet cases: the polarons retained their shape until they approached the line $x_p = x_h$, at which point they began to overlap. The lattice compression associated with the negative polaron and the expansion associated with the positive polaron tended to cancel out when they came into contact, greatly reducing the strength of the interaction between the lattice and the particle-hole pair. In the absence of this coupling, the particle-hole center of mass delocalized along the polymer backbone, while the interparticle degree of freedom remained bound by the Coulomb interaction.

The lattice distortions did not dissipate after coming into contact, but rather passed through each other and continued propagating in the same direction. This is similar to the behavior for solitary waves in nonlinear wave equations,^{36,37} though the profiles of the lattice displacements which emerged from polaron recombination were somewhat distorted, whereas true solitary waves retain their shape exactly. As may be seen from Figs. 3 and 4, the new configuration included a small region of compression bordering and propagating with the expansion, and a small expansion similarly associated with the compression. This pattern of lattice behavior occurred consistently in our simulations. In both the triplet and singlet spin states, a portion of the wave packet remains associated with the lattice distortions, corresponding

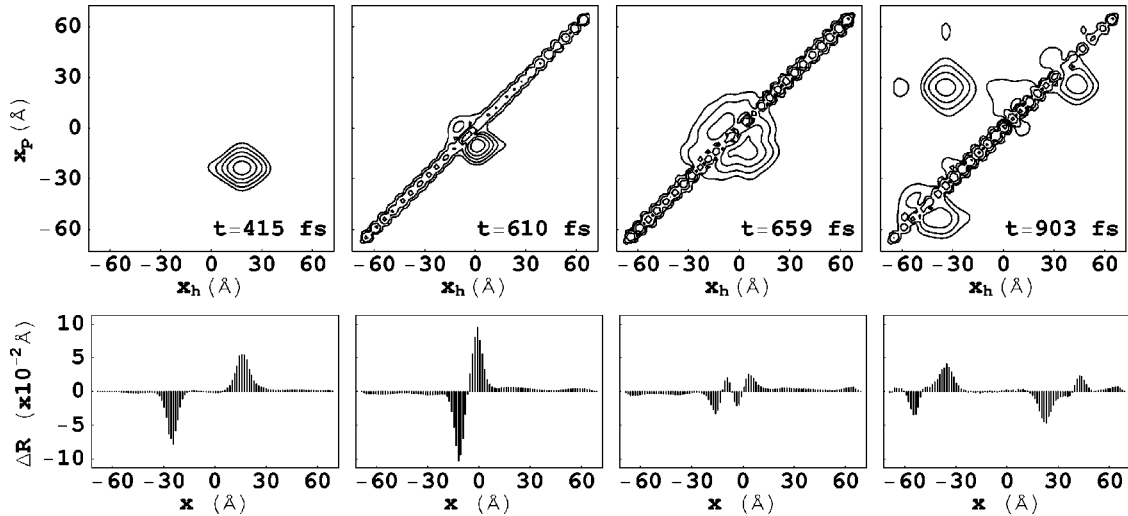


FIG. 3. Triplet state scattering process discussed in Sec. III B. Contour lines are assigned as in Fig. 1.

to components of the polaron wave function which did not scatter into exciton states. However, the majority of the particle-hole amplitude remained in excitonic states and was not associated with the lattice distortions.

To understand the behavior of the wave function during scattering, it is useful to view the lattice motion as driving the evolution of a time-dependent potential energy surface for the quantum degrees of freedom. The transition from polaron to exciton state is then a diabatic process, shown schematically in Fig. 5. The initial polaron wave function is trapped in the state A associated with the potential energy well of the lattice distortion. The relatively high density of states in the translational degree of freedom for the exciton implies that multiple exciton states will lie approximately degenerate to the incident polaron state; we will term this set of states B . When the evolution of the lattice brings the polarons into contact, the energetic barrier between the two wells drops and the eigenstates mix to form a new set of states AB . When the lattice distortions propagate through each other and the polaron potential energy well reemerges in the region $Y < 0$, the states AB are once again split into subsets A and B . The distribution of population between

states A and B will depend on the relative contributions of the states A and B to the character of AB , which will be a function of both the exciton-phonon coupling and the density of states in B .

This interpretation of the dynamics is born out by the behavior of the energy of the quantum degrees of freedom, $E_Q = T_{CM} + V_{QM}$, shown in Fig. 6. The total energy of the quantum wave function follows a similar pattern in both the singlet and triplet states: the energy initially drops slowly as the particle and hole approach each other, corresponding to motion along the gradient of the electric field. Once they are close together (with $E_Q \sim -5000 \text{ cm}^{-1}$), Coulombic interactions take over and the energy drops rapidly. The overlap of the two potential energy wells creates a new AB -mixed state with an energy on the order of -8000 cm^{-1} ; however, the energy rises again as the lattice distortions cancel each other out. In both the singlet and triplet cases, the asymptotic value of E_Q is comparable to the energy of the incident polarons prior to mixing of the states AB . This indicates that the largest contributions to AB come from states B which are most nearly degenerate with A , as expected based on the arguments presented above.

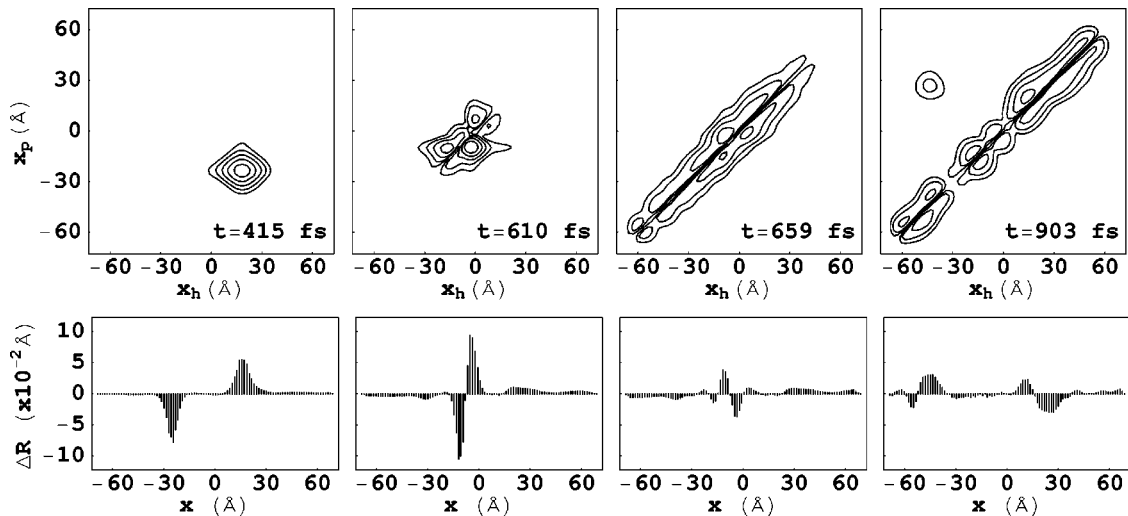


FIG. 4. Singlet state scattering process for Sec. III B. Contour lines are assigned as in Fig. 1.

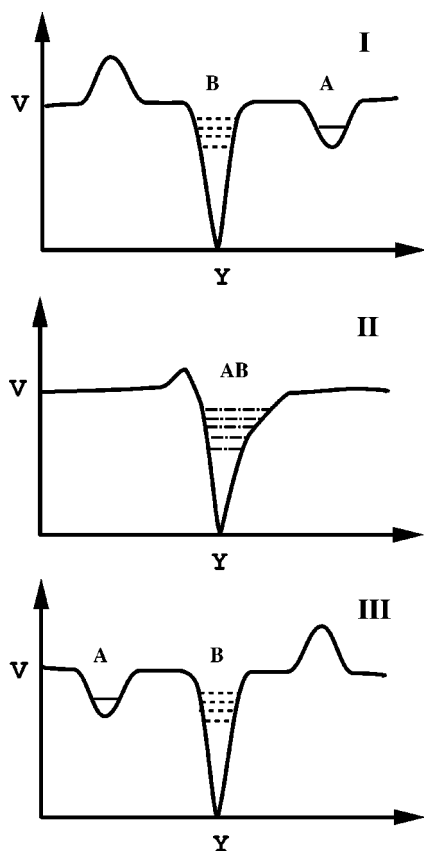


FIG. 5. Schematic description of mixing of polaron and exciton states, as described in the text. Y represents the interparticle distance, and V_{QM} is the quasiparticle potential energy. (I) Prior to scattering, A is the quantum state associated with the well-separated positive and negative polaron pair, and B indicates the exciton states localized near $Y=0$. (II) Scattering begins when positive and negative polarons overlap each other. The polaron and exciton states mix to form the combined states AB . (III) After scattering, the lattice distortions pass through each other and the localized states A and B reemerge. The population distribution between these states is determined by the character of AB .

While the energies of the final state distributions for the singlet and triplet excitons may be similar, they possess quite different dynamical characteristics. The wave function for the triplet state at $t=903$ fs, shown in Fig. 3, possesses a dense nodal structure along the line $x_p=x_h$, indicating a large amount of kinetic energy in the exciton center of mass. In contrast, the singlet wave function shown in Fig. 4 is slowly varying, indicating a much lower translational kinetic energy. Figure 9 shows that this perception is correct: the asymptotic kinetic energy in the triplet state is roughly 2000 cm^{-1} higher than that of the singlet.

To understand the origins of this difference, we consider the nature of the exciton states in the two cases. If one neglects exciton-phonon coupling, the Hamiltonian is separable in the interparticle coordinate $Y=(x_p-x_h)$ and $Z=(x_p+x_h)$.³⁰ The Coulomb potential represents a binding interaction in Y , and the symmetry of the interactions given by Eq. (2.11) implies that even-numbered states will have the correct symmetry for triplet spin states, and odd-numbered states to singlet states. This is consistent with the forms of the exciton wave functions given in Figs. 3 and 4; while

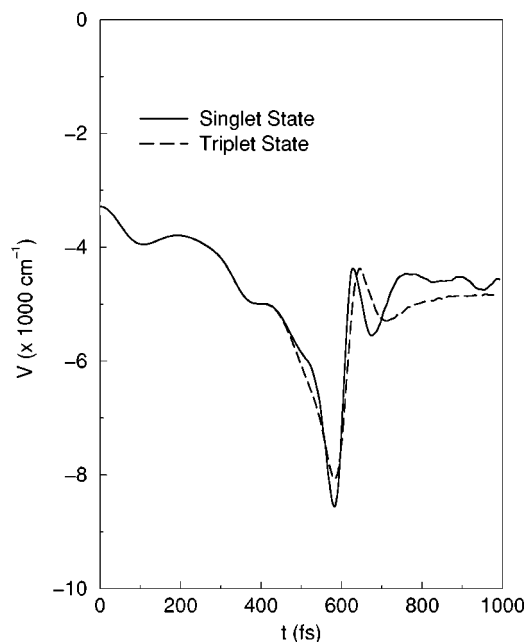


FIG. 6. Total energy (potential and kinetic) for the quantum degrees of freedom for simulation C.

interactions with the lattice and the electric field introduce some asymmetry to the wave function, the singlet state possesses a node at $x_p=x_h$, indicating antisymmetry across that line.

One may take advantage of this approximate separability by writing the wave function in the form

$$\Psi(Y,Z) = \sum_{m,n} c_{mn} \phi_m(Y) \chi_n(Z), \quad (3.2)$$

where $\phi_m(Y)$ are eigenstates of the Coulomb potential and $\chi_n(Z)$ are any complete basis set. While this is only approxi-

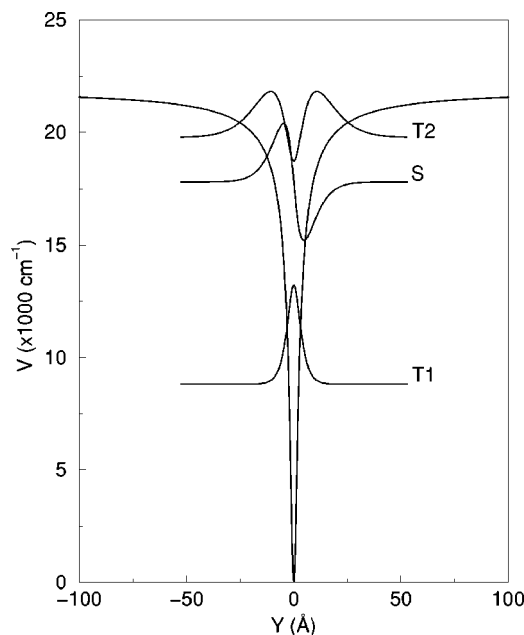


FIG. 7. Ohno potential (assuming favorable exchange interaction) and three lowest-lying eigenstates for parameters from Table I.

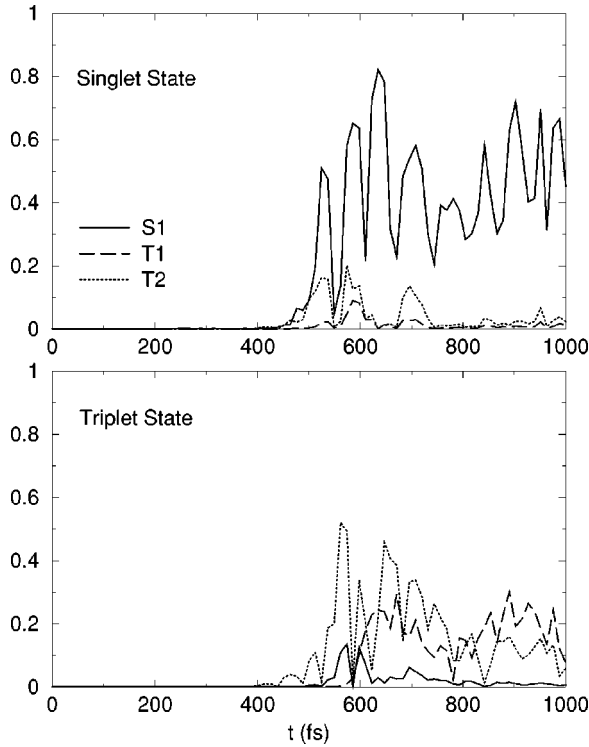


FIG. 8. Projections of the wave function into S , $T1$, and $T2$ for simulation C in the singlet and triplet spin states.

mately true in the total system, we may characterize the exciton states by defining a projection

$$P_m = \int dZ \left| \int dY \phi_m^*(Y) \Psi(Y, Z) \right|^2, \quad (3.3)$$

with $\sum_m P_m = 1$. We use this operator to characterize the wave function $\Psi(Y, Z)$ with respect to its projection in a given state $\phi_m(Y)$. We choose the states ϕ_m to be the eigenstates of the Ohno potential $V_C(Y)$, shown in Fig. 7, allowing us to characterize the exciton state with respect to the assignments of these states given in Ref. 17.

Projections of the wave function into the lowest-lying singlet state S and the two lowest triplets, $T1$ and $T2$, are plotted in Fig. 8. As expected, the S state makes up a sizable fraction of the asymptotic distribution of P_m in the singlet state, while symmetry restrictions prevent the existence of significant populations in $T1$ and $T2$. In the triplet state, S remains virtually unpopulated while $T1$ and $T2$ make significant contributions to the distribution. In each case, the remaining components of the interparticle distribution are made up of higher-lying bound and continuum states of the

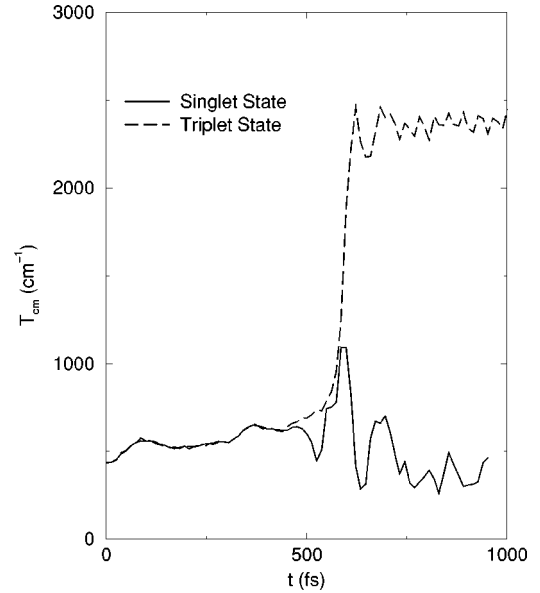


FIG. 9. Kinetic energy of the exciton center of mass as a function of time for the singlet and triplet state in simulation C.

Ohno potential, as interactions with the highly distorted lattice and the electric field lead to probability distributions which are far different from those present in the unmodified Ohno potential.

The energies of the states S , $T1$ and $T2$ for this calculation are given as simulation C in Table III. The relative energies of these three states provide insight into the nature of the scattering process. The S state lies at -4115.8 cm^{-1} ; however, the electric field acts to lower the effective energy of the particle-hole pair by approximately 500 cm^{-1} in the vicinity of the line $x_p = x_h$. Thus, a product state $\Psi(Y, Z) = \phi_S(Y) \chi(Z)$ which is degenerate with the incident polarons at $\sim -4500 \text{ cm}^{-1}$ will possess relatively little kinetic energy in the Z coordinate, as is the case in Fig. 9. In contrast, the energies of $T1$ and $T2$ are substantially different from that of the incident polarons, and the interparticle distribution of the resultant exciton is a mixture of both of these states. The final triplet exciton state also possesses a kinetic energy in Z which is much higher than that of the incident polarons.

The high translational kinetic energy of the triplet exciton implies that the density of states at the energy of the incident polarons is lower than that in the singlet case. To see this, consider that the potential energy surface along the line $Y=0$ is completely flat, bounded at both ends by the hard wall. This implies that to a good approximation the translational degree of freedom of the exciton may be viewed as a particle in a box with energies given by³⁸

TABLE III. Exciton yield as a function of well depth. (The details of C are given in Sec. III B.)

Case.	$U \text{ (cm}^{-1}\text{)}$	$E_{T1} \text{ (cm}^{-1}\text{)}$	$E_{T2} \text{ (cm}^{-1}\text{)}$	γ_T	$E_S \text{ (cm}^{-1}\text{)}$	γ_S	χ_{EL}
A	8778.8	-4232.3	-429.1	0.970	-829.4	0 ^a	0
B	15364	-8513.0	-1165.0	0.754	-2258.7	0.873	0.278
C	21947	-13136.8	-2172.5	0.571	-4153.5	0.968	0.361
D	27434	-17158.9	-3189.5	0.649	-6004.8	0.940	0.326
E	32921	-21293.4	-4347.5	0.967	-8056.3	0.936	0.244

^aSee text for explanation.

$$E_n = \pi^2 \hbar^2 n^2 / (m_{\text{tot}} x_L^2). \quad (3.4)$$

As the energy increases, the energy difference $E_n - E_{n-1}$ increases, lowering the density of states. By the diabatic arguments presented above, this should lead to an overall yield in the triplet exciton which is lower than that of the singlet exciton.

To estimate the exciton yield, we define the exciton to be any bound state where the particle and hole remain within 20 Å of each other, and write the projection operator

$$P_{\text{exc}} = \int dx_p dx_h |x_p, x_h\rangle \langle x_p, x_h| \Theta(20 \text{ \AA} - |x_p - x_h|), \quad (3.5)$$

where $\Theta(x)$ is the Heaviside function. Using the usual identity for projection operators, $P_{\text{exc}} = P_{\text{exc}}^2$ we may evaluate the cross sections for exciton formation in singlet and triplet states

$$\begin{aligned} \gamma_S &= \langle \Psi_S | P_{\text{exc}} | \Psi_S \rangle, \\ \gamma_T &= \langle \Psi_T | P_{\text{exc}} | \Psi_T \rangle. \end{aligned} \quad (3.6)$$

To minimize any artifacts which might arise from the presence of free particle-hole amplitude within this region, we averaged this projection over the last 200 fs of the calculation. For this simulation $\gamma_S = 0.968$ and $\gamma_T = 0.571$, confirming our expectation that the cross section for singlet exciton formation should be substantially larger in the singlet spin state. This leads to $\chi_{\text{EL}} = 36.1\%$ based on Eq. (2.14), which exceeds the purely statistical limit on the quantum yield.

C. Variation of scattering cross section with Coulomb strength

Based on the arguments presented above, γ_S and γ_T should depend strongly on the energies of the states S , $T1$, and $T2$. Since S is near resonance with the incident polaron, a large number of low translational kinetic energy states are resonant with the polaron energy and variation of the the energy E_S should decrease γ_S . On the other hand, since the polaron energy falls between the values of $T1$ and $T2$, one should be able to increase γ_T by tuning the potential parameters to change the energies of these states. Further, the character of the triplet exciton should correspond most closely to the triplet state which is closest to resonance with the incident polaron.

To test these hypotheses, we systematically varied the strength of the Coulombic interaction U as given in Table III, and repeated the calculations with all other parameters held fixed. The calculation reported in Sec. IIIB is included as case C in Table III and will serve as a benchmark in the interpretation of the results of this section. Physically, the parameter $-U$ corresponds to the depth of the Coulomb well. Modifying this parameter would correspond to chemically modifying the polymer system to alter the attractive force between the quasiparticles. The values for U are chosen such that the $T1$ state is nearly resonant with the incident polaron in case A (the lowest value of U), and the $T2$ state is nearly resonant in case E (the highest value). The resultant triplet cross sections, γ_T , given in Table III, are highest when either $T1$ or $T2$ is near resonance with the polaron state, in accordance with our expectations based on the di-

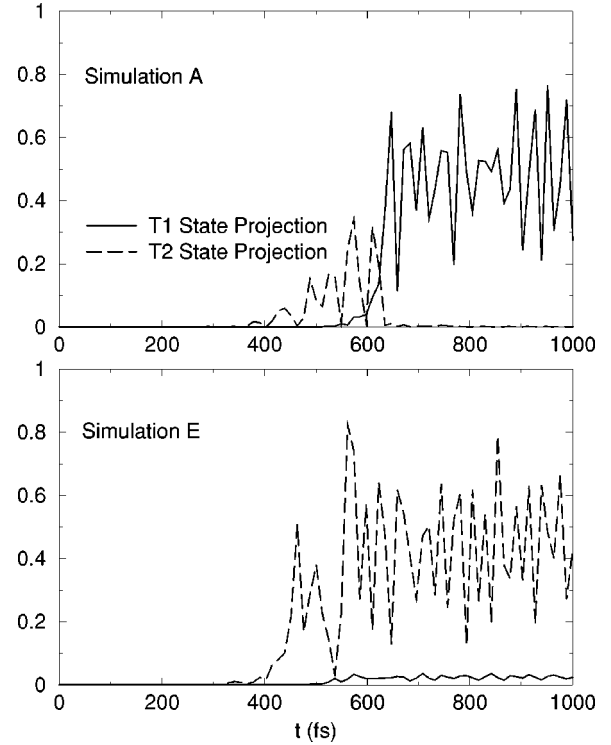


FIG. 10. T1 and T2 projections for simulations A and E as a function of time. The initial rise in T2 in simulation A occurs when the polaron wave packet overlaps the outer lobe of the T2 wave function, and does not represent scattering into that state.

abatic picture discussed above. Further, Fig. 10 indicates that the character of the exciton shifts from predominantly $T1$ to $T2$ as U increases.

With the exception of case A, the singlet cross section γ_S changes by less than 10% with the value of U over the range studied. It follows the predicted pattern, however, in that γ_S decreases as the state moves out of resonance with the polaron state. The relatively small change in the magnitude of γ_S may stem from the higher density of states in the singlet degrees of freedom. As discussed above, the even-numbered states of the Ohno potential must correspond to a triplet configuration, while the odd-numbered states to a singlet. The energy difference between adjacent quantum states of the Ohno potential decreases as the energy approaches the dissociation threshold, and since $T1$ always lies below S , the density of states in the triplet manifold is always lower than that in the singlet manifold. The higher density of states increases the probability of scattering into a singlet state, making γ_S robust with respect to changes in singlet state energy.

Case A is an exception to this trend, owing to the existence of an unusual phenomenon. The dynamics of this simulation are depicted in Fig. 11: Here, the polarons approach the $x_p = x_h$ region normally, but rather than scattering into an exciton state, the polarons simply stop translating as they come into contact. They form an apparently stable peak in the wave function associated with a distortion of the lattice, and while the width of these features oscillates in time, the center does not move.

This structure comes about because for the value of U employed in this particular case, the energy of the S state is higher than the energy of the incident polarons. Scattering

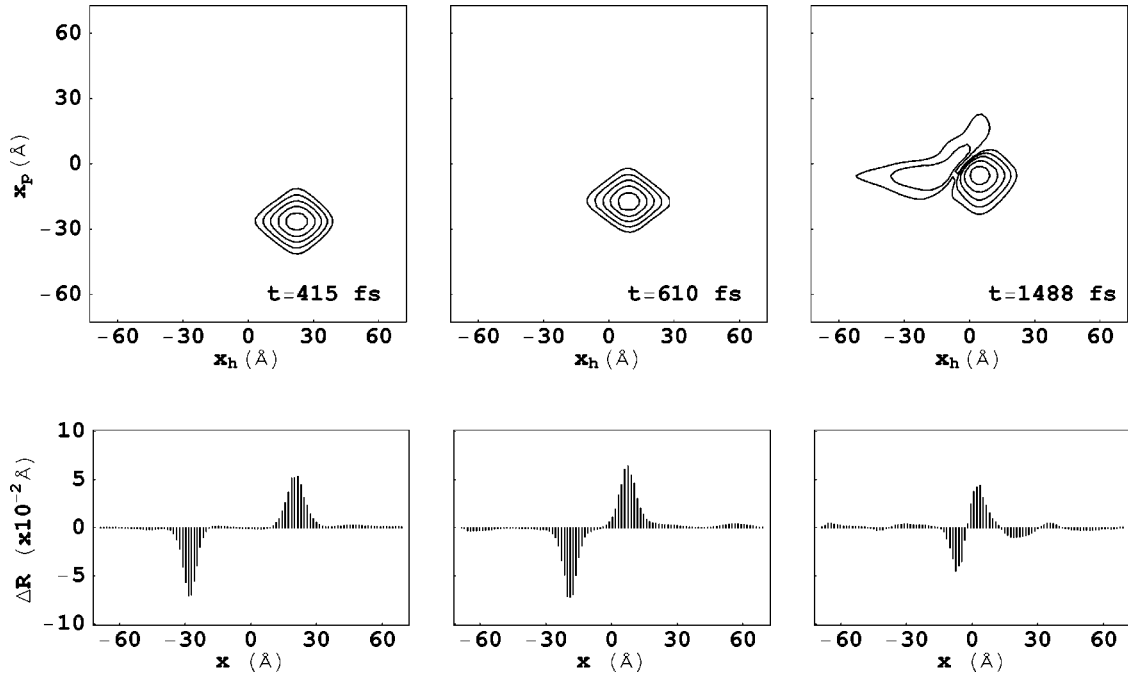


FIG. 11. Singlet state scattering process for simulation A. Contour lines are assigned as in Fig. 1.

into an exciton state would therefore require an input of energy, and cannot take place in the absence of thermal excitation. Energetically, the most favorable process would be for the polarons to pass through each other and continue propagating along the gradient of the electric field. But the lattice compression associated with the negative polaron and the expansion associated with the positive polaron would cancel each other out during such a process, increasing the energy of the quasiparticles. Thus, there is an energetic barrier to such a transition, and the peaked structure in Fig. 11 represents a metastable state.

We determine the characteristics of this state by taking the configuration of the singlet state propagation at time $t = 1000$ fs and relaxing it according to the scheme outlined in Sec. III A. For this relaxation, we take $U=0$ but retain the nonzero value for the electric field \mathcal{E} given in Table I. The structure converges to the local minimum, the properties of which are reported in Table IV.

We know of no analogous structure reported in the literature. Superficially, one might view this state as similar to the ‘‘breather’’ modes of polyacetylene,^{39,40} in that both types of motion involve an oscillatory lattice motion coupled to a localized electronic excitation. In our case, however, the stabilization of the motion is brought about by a competition between the action of the external electric field (which drives the polarons through each other) and the quasiparticle-lattice coupling (which prevents the overlap of the polarons). Breathers in polyacetylene are independent of any external field.

It is difficult to assess the likelihood of observing such structures in physical systems. While the phenomena responsible for their existence are certainly present experimentally, these structures may be very unstable in the presence of perturbations not included in this calculation. Without knowing the magnitude of the energetic barrier preventing the two polarons from passing through each other, we cannot estimate the lifetime of such a bound structure at finite tempera-

ture. Likewise, while spin-orbit coupling is negligible on the timescale of this calculation, the system would eventually cross to the triplet manifold and make a transition to the $T1$ exciton state.

The experimental observation of such a structure would seem to be a significant challenge. The state would likely be nonemissive, as the relatively large interparticle distance would prevent recombination of the particle and hole. It might be detected via absorption, as there may be higher-lying electronic states which are photoaccessible from this state, but we cannot assess the likelihood of this situation within the context of the present model. It would also be inconvenient to look for such structures experimentally, as it would require the construction of a device equivalent to photodiode from a polymer which is neither photonor electroluminescent. Thus, we can neither dismiss the existence of such states as an artifact of our method nor suggest a well-defined approach by which their existence could be confirmed.

D. Variation of the electric field

The most readily variable potential energy parameter in experimental LED systems is the electric bias applied across

TABLE IV. Metastable configuration of polarons in the absence of the Coulombic interaction. $\langle H \rangle$ contains the effect of the electric field. Values for the polaron configuration in Table II are taken in the absence of the electric field, as the interparticle distance of the polaron state is not fixed. In our simulations, this pair of ‘‘locked’’ polarons lies 354.1 cm^{-1} below the initial polaron configuration in the presence of the electric field.

RMS interparticle distance	17.6 Å
Standard deviation	13.7 Å
$\langle H \rangle$	-1489.4 cm^{-1}
$\langle T \rangle$	1167.1 cm^{-1}
$\langle V_{\text{ph-latt}} \rangle$	-4567.2 cm^{-1}
$\langle V_{\text{lat}} \rangle$	2290.3 cm^{-1}

TABLE V. Exciton yield as a function of electric field strength. With the exception of the external electric field \mathcal{E} , all parameters are assigned as in Table I.

	\mathcal{E} (eV/Å)	γ_T	γ_S	χ_{EL}
\mathcal{E}_0	0	0.707	0.979	0.316
\mathcal{E}_1	-8.919×10^{-4}	0.571	0.968	0.361
\mathcal{E}_2	-1.7838×10^{-3}	0.611	0.957	0.343

the polymer LED device. The electric field controls many parameters related to charge carrier density and mobility,^{10,11,12} but here we focus exclusively on its role in an individual scattering event. To this end, we carry out simulations of the scattering process at varying strengths in the electric field. Simulation \mathcal{E}_1 in Table V is the benchmark simulation discussed in Sec. III B; only two other simulations were carried out, as the polarons in this model become unstable when $\mathcal{E} \sim 4.5 \times 10^{-3}$ eV/Å ($5 \times$ the value of \mathcal{E} reported in Table I). The results, tabulated in Table V, indicate that the yield in the singlet state varies little with electric field strength, decreasing slightly with increasing \mathcal{E} . In contrast, the triplet yield drops substantially when the field is turned on, but increases slightly as the field is increased.

To interpret this behavior, we must understand how the electric field affects the dynamics of the system. While the presence of the electric field will lead to a small change in the energies of the quantum states, this effect will not be very important as the widths of the polaron and exciton states are small so that the potential does not vary greatly over this domain. A more important effect is in the energy of the incident polaron pair: the stronger the electric field, the more energy will be associated with the motion of the polaron pair.

Increasing the electric field increases the potential energy associated with the initial polaron configuration, and within the context of the simulation this increases the total energy in the system. The energy of the polaron pair interacting with the electric field is given by

$$V_{\text{field}} = \int dx_p dx_h \psi^*(x_p, x_h) \psi(x_p, x_h) \times [V_e(x_h) - V_e(x_p)] - V_{f0}, \quad (3.7)$$

where V_{f0} is the interaction energy at time zero (i.e., $V_{\text{field}} = 0$ at time 0). As the propagation progresses, the polarons move along the gradient of the electric field and V_{field} decreases. As shown in Fig. 12, the slope of the initial rise in the kinetic energy of the lattice nearly matches the slope of $|V_{\text{field}}|$, indicating that the energy of the field is almost entirely taken up in the motion of the lattice. This implies that changes in the motion of the lattice will determine the changes in the dynamics with varying field strength. Figure 13 bears out this interpretation: the large drop in quantum energy associated with the particle-hole collision occurs at earlier times in the presence of a strong electric field, indicating a more rapid collision. The drop is also larger in the presence of the electric field; indeed, the singlet state in the absence of the electric field shows almost no drop in energy. The lattice dynamics affect the shape of the potential energy surface experienced by the particle-hole pair when the po-

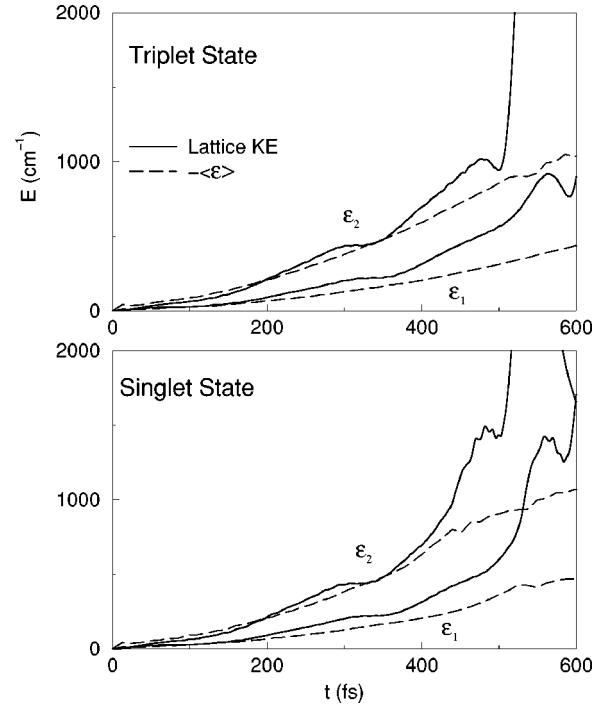


FIG. 12. Data for simulation \mathcal{E}_1 and \mathcal{E}_2 . **Solid:** Lattice kinetic energy as a function of time. **Dashed:** $|V_{\text{field}}|$ as a function of time. See text for discussion.

larons overlap (the AB configuration in Fig. 5), which will affect the nature of the mixing with exciton states. The details of this mixing are unclear. Thus it is not obvious how variation of the electric field will affect the quantum yield for a given set of parameters.

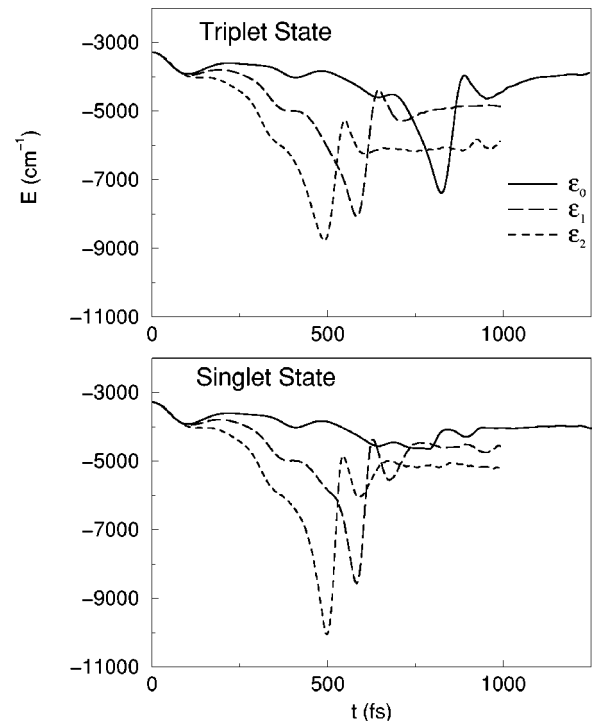


FIG. 13. Total energy (potential and kinetic) for the quantum degrees of freedom as a function of time for varying electric field strengths.

TABLE VI. Exciton yield as a function of quasiparticle mass. With the exception of the effective masses m_p and m_h , all parameters are assigned as in Table I.

m_p (emu)	m_h (emu)	γ_T	γ_S	χ_{EL}
2	1	0.900	0.994	0.259
1	2	0.790	0.900	0.275
1	1	0.571	0.968	0.361
1/2	1	0.324	0.912	0.484
1	1/2	0.193	0.842	0.593

E. Variation of the effective masses of the particle and hole

The masses of the particle and hole used in these calculations are effective masses, which are determined by the interaction between the the excited electron (or vacancy in the valence band) and the valence electrons which surround it.⁴¹ As such, these masses vary with the electronic structure of the polymer, and may be altered by chemical derivatization of a given polymer.

We employed five different combinations of effective masses in this work, reported in Table VI. We have already discussed in the preceding sections of this paper how the relative energies of the polaron and exciton levels affect the dynamics. The exciton energy levels are primarily dependent on the energies E_S , E_{T1} and E_{T2} , which in turn are dependent on the reduced mass of the particle-hole pair $\mu = m_p m_h / (m_p + m_h)$. We may therefore eliminate the resonance effect by comparing simulations with different quasiparticle masses, but identical reduced masses. This principle guided the choice of the masses used in our simulations.

Alteration of the quasiparticle masses necessarily alters the structure of the polarons. The initial polaron configurations for each set of effective masses were recalculated using the procedure in Sec. III A. The results for simulations employing the new parameters are tabulated in Table VI, and the case where the total mass $m_{tot}=2$ corresponds to the benchmark calculation carried out in Sec. III B. The resultant cross sections indicate that the yield is insensitive to the relative masses of the two quasiparticles, but depends strongly upon the total mass. For the simulations in which $m_{tot}=3$, the yield in the singlet state is virtually independent of the relative mass, while yield in the triplet state changes by 11%. For $m_{tot}=1.5$ emu, changing the relative masses of the particle and hole change the singlet yield by 7%, and the triplet yield by 13%. The change is due to the change in the configuration in the exciton; for $m_p > m_h$, the compressed region of the lattice is narrower than the region of expansion, and vice versa for $m_p < m_h$. This affects the form of the potential energy surface experienced by the quasiparticles as the polarons come into contact, which naturally affects the reaction cross section.

This effect is far less significant than the change in dynamics associated with the change in the total mass, however. Where increasing the total mass increased the yield in both the singlet and triplet states, decreasing the overall mass decreased the yield in both states, but reduced the triplet yield to a far greater degree than the singlet. Indeed, χ_{EL} is by far the largest of any of our simulations when $m_{tot}=1.5$. The reason for this dependence on m_{tot} stems from the den-

sity of states in the translational degree of freedom for the exciton. The mass dependence of the translational energy eigenstates given in Eq. (3.4) makes this clear: as the mass of the particle-hole pair decreases, the density of states decreases, reducing the reactive cross section. Further, this effect is most important at higher translational energies, where the density of states is lowest, and the high translational kinetic energy associated with the triplet exciton makes γ_T more sensitive to the total mass than γ_S . Thus, by lowering the total effective mass of the exciton, we sacrifice absolute cross section in the singlet state exciton, but gain in the quantum efficiency χ_{EL} .

IV. CONCLUSIONS

We have simulated the scattering of positive and negative polarons into both singlet and triplet excitons, and have shown that the process may be readily understood in a diabatic representation of the electronic degrees of freedom. The dynamics of recombination hinge on the mixing of exciton and polaron quantum states at the time when the polarons begin to overlap with each other, and the reactive cross section is primarily a function of the density of exciton states near resonance with the incident polaron quantum state. This density of states is sensitive to the strength of the Coulombic interaction between the particle and hole pair, and the effective masses of the quasiparticles. We also find that at the microscopic level discussed here, χ_{EL} , is relatively insensitive to the strength of the applied voltage.

The most important aspect of this work is the calculation of the cross sections γ_S and γ_T , which demonstrate that the statistical limit of $\Phi_{EL} = 1/4\Phi_{PL}$ is invalid. Indeed, the analysis of the mechanism for polaron scattering observed here may be used to develop a strategy to assist in the search for highly efficient electroluminescent materials. While in general $\Phi_{EL} \neq \chi_{EL}$ in real devices, optimization of χ_{EL} is one route to improving the electroluminescence yield in devices, and our work suggests ways in which this may be accomplished.

The first parameter to consider in such a problem is the energy of the lowest-lying singly-excited singlet relative to the quasiparticle energy of the incident polarons. This is not the exciton binding energy, which contains contributions from the vibrational degrees of freedom, but rather the energy of the localized electronic excitation associated with the distortion of the lattice. This quantity is not readily accessible experimentally, and it seems likely that some level of theory must be employed in estimating how those energies will change on derivatization of the polymer. However, our simulations have shown that the yield in the singlet state is comparatively insensitive to the exact value of the energy, so long as the singlet state lies reasonably close to the polaron-quasiparticle energy.

Another consideration is the energies of the two lowest-lying singly-excited triplet states. Once the energy of the singlet state has been tuned to the desired level, the ideal configuration would increase the energy gap between the singlet state and each of the two neighboring triplet states. This would move the triplet states further out of resonance with the polaron pair, decreasing the triplet cross section. This is not likely to be necessary, however, as the energy gap be-

tween neighboring states is typically substantial: in poly(paraphenylene vinylene) (PPV), the difference in energy between the lowest-lying singlet and triplet exciton states is $\sim 8000 \text{ cm}^{-1}$. This is comparable to the size used in our benchmark simulation C, which depending on other factors can provide a favorable χ_{EL} .

The most significant factor in increasing χ_{EL} , however, is the effective mass of the exciton. Assuming the singlet exciton state is near resonance with the quantum energy of the polaron, the states accessible via scattering into the triplet exciton must possess a high translational kinetic energy. The triplet scattering process is therefore more sensitive to the density of states in the translational degree of freedom, and when this is lowered by reducing the effective mass of the exciton, χ_{EL} increases. The effective masses are readily accessible to theoretical treatments, as they simply represent deviations from the ideal dispersion relationship in the relevant electronic band.⁴¹ In essence, the effective mass of a quasiparticle is the inertia associated with the reorganization of σ and π electron cloud as the quasiparticle propagates along the chain. This parameter is controlled by the polarizability of the polymer and its surroundings, and therefore represents a controllable parameter.

Altering the parameters discussed above requires choosing an appropriate class of polymer and derivatizing it to tune the parameters. Our own work assumes the polymer to be composed entirely of C-H monomers, but the principle features of the phenomena observed here should apply in more complicated systems so that the strategies devised here will still be relevant. One specific strategy for control of particle-hole interaction parameters is suggested by the work of Gartstein, Rice, and Conwell.^{24,42} The authors have studied the nature of the electron-hole interaction in phenylene-based polymers using a model based on the symmetry of the phenylene subunit. Their work demonstrates that the parameters describing the interaction of the particle-hole pair are influenced by the local symmetry of the monomer, and derivatization may significantly influence the quasiparticle interaction by altering this symmetry.⁴² This suggests a means of

altering the relative and absolute energies of the singlet and triplet states through chemical derivatization, as discussed above.

Another route is suggested by the work of Yaron and co-workers,^{43,44} who have studied the influence of the electronic polarization of neighboring polymer chains on particle and hole behavior. The authors find that the polarization of the surrounding media has a dramatic impact on the energy of the asymptotically separated particle and hole, and can strongly influence the effective mass of the quasiparticles. It is worth noting that the theoretical treatment of the problem predicts that the influence of the surrounding media should be smallest as the system approaches the exciton limit, so it is unclear how significant the impact of the surrounding media should be on the polaron scattering process. Likewise, the probability of a polaron-polaron collision in the bulk polymer is influenced by the dielectric constant for the medium,¹² so processes which increase χ_{EL} may lower the total efficiency Φ_{EL} . Nevertheless, variation of the polarizability of the polymer medium may be one route to optimization of electroluminescence quantum efficiency.

The model presented here is an idealized model for a polymer with a nondegenerate ground state. While it clearly lacks crucial physical and geometric features present in actual polymeric systems, the model captures the salient and ubiquitous dynamical features of the recombination process, namely: electron-phonon coupling and particle/hole correlation. Thus, our treatment provides dynamical insight into the process of polaron recombination. The strategies suggested here may be combined with knowledge of the frequency of polaron collision within the bulk polymer,⁹⁻¹² and the subsequent dynamics associated with the return to the ground electronic state⁵ to provide insight into the utility of a given polymer for use in organic LED's.

ACKNOWLEDGMENTS

Funding for this work was provided by the National Science Foundation (CHE-9984416), and the R. A. Welch Foundation (E-1337).

*Present address: Department of Chemistry, Pennsylvania State University, University Park, PA 16802.

¹J. Burroughes, D. Bradley, A. Brown, R. Marks, K. MacKay, R. Friend, P. Burns, and A. Holmes, *Nature (London)* **347**, 539 (1990).

²D. Braun and A. Heeger, *Appl. Phys. Lett.* **58**, 1982 (1991).

³D. Bradley, *Synth. Met.* **54**, 401 (1993).

⁴P. Ho, D. Thomas, R. Friend, and N. Tessler, *Science* **285**, 233 (1999).

⁵A. Burin and M. Ratner, *J. Chem. Phys.* **109**, 6092 (1998).

⁶F. Garten, A. Hilberer, F. Cacialli, E. Esselink, Y. van Dam, B. Schlattmann, R. Friend, T. Klapwijk, and G. Hadziioannou, *Adv. Mater.* **9**, 127 (1997).

⁷W.-L. Yu, J. Pei, Y. Cao, W. Huang, and A. Heeger, *Chem. Commun. (Cambridge)* **1999**, 1837.

⁸A. Holmes, B. Chuah, X.-C. Li, F. Cacialli, J. Morgado, H. Siringhaus, D. D. Santos, S. Moratti, J.-L. Brédas, R. Friend, and F. Garnier, *Proc. SPIE* **3476**, 24 (1998).

⁹F. S. J. Staudigel, M. Stössel, and J. Simmerer, *J. Appl. Phys.* **86**, 3895 (1999).

¹⁰H. Bässler, *Polym. Adv. Technol.* **9**, 402 (1998).

¹¹U. Albrecht and H. Bässler, *Chem. Phys.* **199**, 207 (1995).

¹²Y. Gartstein, E. Conwell, and M. Rice, *Chem. Phys. Lett.* **249**, 451 (1996).

¹³Y. Cao, I. Parker, G. Yu, C. Zhang, and A. Heeger, *Nature (London)* **397**, 414 (1999).

¹⁴I. Frank, J. Hutter, D. Marx, and M. Parrinello, *J. Chem. Phys.* **108**, 4060 (1998).

¹⁵K. Thompson and T. Martinez, *J. Chem. Phys.* **110**, 1376 (1999).

¹⁶B. Hartke and E. Carter, *J. Chem. Phys.* **97**, 6569 (1992).

¹⁷M. Kobrak and E. Bittner, *J. Chem. Phys.* **112**, 5399 (2000).

¹⁸K. Cho, in *Excitons*, edited by K. Cho (Springer-Verlag, New York, 1979), pp. 1-13.

¹⁹This is different from the case of two electrons due to the time-reversal symmetry element associated with the hole. See J.-P. Blaizot and G. Ripka, *Quantum Theory of Finite Systems* (MIT Press, Cambridge, MA, 1986).

²⁰L. D. Landau and E. M. Lifshitz, *Quantum Mechanics*, 3rd ed. (Pergamon, New York, 1991), Sec. 62.

²¹E. Conwell and M. Wu, *Appl. Phys. Lett.* **70**, 1867 (1997).

- ²²U. Sum, K. Fesser, and H. Büttner, *Phys. Rev. B* **38**, 6166 (1988).
- ²³K. Fesser, U. Sum, and H. Büttner, *Phys. Rev. B* **44**, 421 (1991).
- ²⁴Y. Gartstein, M. Rice, and E. Conwell, *Phys. Rev. B* **51**, 5546 (1995).
- ²⁵P. Lane, X. Wei, Z. Vardeny, J. Poplawski, E. Ehrenfreund, M. Ibrahim, and A. Frank, *Chem. Phys.* **210**, 229 (1996).
- ²⁶T. Kobayashi, M. Yasuda, S. Okada, H. Matsuda, and H. Nakanishi, *Chem. Phys. Lett.* **267**, 472 (1997).
- ²⁷D. McClure, *J. Chem. Phys.* **20**, 682 (1952).
- ²⁸R. Kosloff, *J. Phys. Chem.* **92**, 2087 (1988).
- ²⁹T. Park and J. Light, *J. Chem. Phys.* **85**, 5870 (1986).
- ³⁰M. Kobrak and E. Bittner, *J. Chem. Phys.* **112**, 5410 (2000).
- ³¹W. Su and J. Schrieffer, *Proc. Natl. Acad. Sci. U.S.A.* **77**, 5626 (1980).
- ³²A. Takahashi, *Phys. Rev. B* **54**, 7965 (1996).
- ³³A. Takahashi, *Phys. Rev. B* **56**, 3792 (1997).
- ³⁴The energy of the free particle-hole pair is taken to be the minimum energy configuration for an asymptotically separated particle and hole pair interacting with the vibrational lattice in its equilibrium geometry. It is determined in these simulations via imaginary time propagation of the quantum degrees of freedom on a frozen lattice, in the absence of any Coulombic interaction between the particle and hole.
- ³⁵S. Yaliraki and R. Silbey, *J. Chem. Phys.* **104**, 1245 (1996).
- ³⁶H. Goldstein, *Classical Mechanics*, 2nd ed. (Addison-Wesley, Reading, MA, 1980).
- ³⁷Solitary waves of this type are often referred to as “solitons,” but we do not use the term here to avoid confusion with topological solitons such as those discussed in A. Heeger, S. Kivelson, J. Schrieffer, and W.-P. Su, *Rev. Mod. Phys.* **60**, 781 (1988).
- ³⁸E. Merzbacher, *Quantum Mechanics*, 2nd ed. (Wiley, New York, 1970).
- ³⁹A. Bishop, D. Campbell, P. Lomdahl, B. Horovitz, and S. Phillipot, *Phys. Rev. Lett.* **52**, 671 (1984).
- ⁴⁰W. Wang, J. Gammel, A. Bishop, and M. Salkola, *Phys. Rev. Lett.* **76**, 3598 (1996).
- ⁴¹P. Yu and M. Cardona, *Fundamentals of Semiconductors* (Springer, New York, 1996).
- ⁴²Y. Gartstein, M. Rice, and E. Conwell, *Phys. Rev. B* **52**, 1683 (1995).
- ⁴³E. Moore, B. Gherman, and D. Yaron, *J. Chem. Phys.* **106**, 4216 (1997).
- ⁴⁴E. Moore and D. Yaron, *J. Chem. Phys.* **109**, 6147 (1998).